Construction and Building Materials 414 (2024) 135062

Contents lists available at ScienceDirect

Construction and Building Materials

journal homepage: www.elsevier.com/locate/conbuildmat

Understanding roles and evaluating reactivity of fly ashes in calcium aluminate binders

Sai Akshay Ponduru [a], Taihao Han [a], Jie Huang [b], Narayanan Neithalath [c], Gaurav Sant [d], Aditya Kumar [a,*]

[a] Department of Materials Science and Engineering, Missouri University of Science and Technology, Rolla, MO 65409, USA
[b] Department of Electrical and Computer Engineering, Missouri University of Science and Technology, Rolla, MO 65409, USA
[c] School of Sustainable Engineering and the Built Environment, Arizona State University, Tempe, AZ 85287, USA
[d] Department of Civil and Environmental Engineering, University of California Los Angeles, CA 90095, USA

ARTICLE INFO

Keywords:
Fly ash
Calcium aluminate cement
Compressive strength
Hydration kinetics
Reactivity

ABSTRACT

Calcium aluminate cement (CAC) is an alternative to Portland cement, valued for its superior early strength and thermal resistance. Partially replacing CAC with Fly ash (FA) can reduce carbon footprint and production costs of CAC, producing sustainable cementitious binders. This research investigates on various properties (i.e., hydration kinetics; phase assemblage evolution; compressive strength) of [CAC + FA] binders. Using 13 distinct FAs, up to 50% of CAC was substituted. The study measures hydration kinetics, compressive strength, and employs the *number of constraints* to estimate FA reactivity. Advanced quantitative analysis draws links between hydration kinetics and compressive strength and elucidate the role of FA (including composition and reactivity) on binder performance. Techniques such as X-ray diffraction and thermodynamic modeling illuminate phase compositions in [CAC + FA]. This study also develops a novel method that evaluates the degree of reaction of FA in non-Portland cement binders. Then the correlation between degree of reaction of FAs at 3 days *number of constraints* is revealed.

1. Introduction

Concrete, predominantly made from Portland cement (PC), ranks as the most utilized construction material worldwide. This massive production of PC is responsible for nearly 8% of global CO_2 emissions induced by human activities [1,2]. The bulk of these emissions stem from the energy-intensive manufacturing processes and the decarbonization of limestone in clinker production [3,4]. To counteract these environmental repercussions, there are two primary strategies: introducing industry wastes [e.g., slag, fly ash (FA), waste glass, etc.] to partially replace PC; and adopting alternative cement. Calcium aluminate cement (CAC) stands out as an eco-friendlier substitute to PC [5,6]. Notably, CACs are heralded for their lower carbon emissions during production, with studies indicating a substantial 47% reduction in CO_2 emissions compared to PC [7]. CAC possess several remarkable properties, including excellent early strength, significant resistance to acids, ability to withstand high temperatures, and impressive abrasion resistance [5,8].

In CAC, the major components are CA, CA_2, and $C_{12}A_7$, with their distribution contingent upon the specific ratio of CaO to Al_2O_3 (as denoted by cement chemistry notations: C = CaO; A = Al_2O_3; S = SiO_2; \$ = SO_3; and H = H_2O). During hydration, the calcium to aluminum ion molar ratio in the pore solution hovers around 0.55 to 0.6 [9,10]. This leads to the crystallization and precipitation of metastable calcium-aluminate-hydrate phases (e.g., CAH_{10}, C_4AH_{13} or C_4AH_{19}, and C_2AH_8) on the cement particle surface [9,11]. Based on temperature, the initially formed hydrates (i.e., CAH_{10} and C_2AH_8) transfer into their stable counterpart (i.e., C_3AH_6). At low temperatures ($T \leq 20$ °C), CAH_{10} is the dominant hydration product. At moderate temperatures (20 °C $\leq T <$ 35 °C), C_2AH_8 and AH_3 are the major phases form during hydration. However, at latter stages or higher temperatures ($T \geq 35$ °C), these phases transfer into denser C_3AH_6 and AH_3 phases [5,9,12]. This phase transition results in increased porosity and a corresponding decline in compressive strength [13,14].

The broader adoption of CAC is hindered by several challenges, most notably its economic feasibility. The production of CAC typically

* Correspondence to: Department of Materials Science and Engineering, Missouri University of Science and Technology, B49 McNutt Hall, 1400 N Bishop, Rolla, MO 65409, USA.
E-mail address: kumarad@mst.edu (A. Kumar).

https://doi.org/10.1016/j.conbuildmat.2024.135062
Received 1 November 2023; Accepted 14 January 2024

involves the use of high-cost raw materials such as bauxite. Though the alumina is available in earth's crust in the form of feldspar and clay, the source for high grade alumina i.e., bauxite is not widely available. Given these economic and environmental obstacles, research is being channeled towards exploring feasible solutions that can make CAC more accessible for broader applications. One potential approach involves the use of supplementary cementitious materials (SCMs) to partially replace CAC. FA can be used to partially substitute CAC. Global statistics reveal an abundant production of FAs, with an estimated 800 million tons being generated annually [15,16]. This substantial volume keeps growing, with forecasts projecting that the global FA production will likely exceed 1.04 billion tons by the year 2030 [17]. However, despite such large-scale production, the global recycling rate of FAs remains disappointingly low. Over the years, it has seen only a marginal increase, rising from 16% to a meager 25% of the total production [18–20]. This stark data underscores a disconcerting reality - a significant proportion of FA is not recycled but discarded into landfills. This waste management issue is rampant across numerous regions globally and it poses severe risks to the environment. The disposal of FA in landfills contributes to water contamination, releases harmful gases, and adds to the overall carbon footprint [16,17]. In light of these facts, the utilization of FA as a partial substitute for CAC offers a sustainable approach by reducing negative environmental impact caused by CAC and FA.

Owing to its highly inconsistent batch-to-batch composition, FA demonstrates complex influences on the hydration and mechanical properties of CAC. The major components of FA are SiO_2, Al_2O_3, and CaO. In [CAC + FA] biner, the CaO and SiO_2 in FA—if soluble—can react with hydration products (i.e., CAH_{10} and C_2AH_8) to form straetlingite (C_2ASH_8) [14,21], a space-filling and stable hydration product. This bypasses—to a certain degree—the conversion of CAH_{10} and C_2AH_8 (metastable phases) to C_3AH_6, and prevents the reduction of compressive strength (i.e., due to conversion-induced porosity increase, as discussed above) [22]. Usually, FA contains SO_3 less than $1\%_{mass}$; thus, exerting negligible effect on the hydration of CAC or the hydration products. However, bottom and off-specification FA, or FAs produced from combustion of high-sulfur coal sources, can have up to $20\%_{mass}$ SO_3 [23]. Previous studies have shown that SO_3 (released from FA as SO_4^{2-}) can react with anhydrous CaO and Al_2O_3 phases of CAC (or FA), leading to the formation of ettringite, and subsequently monosulfoaluminate [21,24,25]. The additional ettringite substantially reduces the amount of calcium aluminate hydrates; furthermore, the transformation from ettringite to monosulfoaluminate at later ages (after SO_3 is depleted) results in reduction of porosity and pore-connectivity of the binder [21]. Likewise, and as stated above, the release of CaO and SiO_2 from FAs—as Ca^{2+}, $H_2SiO_4^{2-}$, and/or $H_3SiO_4^-$—can result in the conversion of calcium aluminate hydrates (CAH_{10} and C_2AH_8) to straetlingite (C_2ASH_8); thus, entirely bypassing the conversion of these *metastable* calcium aluminate hydrates to hydrogarnet (C_3AH_6).

Many studies have investigated the impacts of FA on the properties of CAC binders. Lopez et al. [26] have applied scanning electron microscopy and mid and near-infrared spectroscopy to study the microstructure of [CAC + FA] binders. Pacewska et al. [27] have used calorimetry and thermal analysis to describe the hydration kinetics of CAC partially substituted by FAs ($<25\%_{mass}$). Auer et al. [28] have found that, in [CAC + FA] binders, SO_3-rich FAs result in the formation of ettringite (at early ages) and monosulfoaluminate (at later ages) instead of calcium aluminate hydrates. Previous studies have successfully revealed the hydration products of [CAC + FA] binders; that said, these studies have not provided comprehensive understandings of the influence of FA on CAC's hydration kinetics and mechanical properties. Moreover, each study focused on just limited numbers of FAs—in general, just one or two—resulting in an incomplete understanding of the impacts of a wide range of chemical compositions of FAs. Furthermore, in most FAs, the SO_3 content is lower than $1\%_{mass}$; therefore, it is still unclear whether—and how—the SO_3 affects hydration kinetics and mechanical properties of CAC binders. These knowledge-gaps result, mainly, from our lack of understanding of the reactivity of FAs in [CAC + FA] binders. Researchers have used ASTM C618 [29] to classify the aqueous reactivity of FAs solely according to the calcium content. However, prior studies [30–32] have indicated that this ASTM standard is too simplistic to comprehensively and accurately quantify the aqueous reactivity of FAs. This is because FAs are highly heterogeneous, multi-component materials, wherein the amorphous phase content varies over a wide range ($50\text{-to-}90\%_{mass}$ [30,33,34]), and these variations cannot be explicitly accounted for in the ASTM standard. Topological constraint theory (TCT) [30,35–37] can be employed to estimate the reactivity of FAs. The core premise of TCT utilizes the chemical composition of FAs to generate a unique chemo-structural parameter [*number of constraints* (n_c)]. This parameter can be used as a proxy to present the reactivity of FAs.

In this research, we employed 13 different types of FAs to partially replace CAC in binders. The replacement level of FAs—including those containing up to $4\%_{mass}$ of SO_3—is varied from $10\%_{mass}$ to $50\%_{mass.}$ Our study focused on assessing how these FAs impacted both the compressive strength and hydration kinetics of the [CAC + FA] binders. Additionally, our research aimed to establish correlations between the reactivity of FAs (expressed as *number of constraints*) and properties (i.e., hydration kinetics; compressive strength; and phase assemblage). Furthermore, to gain a deeper understanding, we analyzed the phase assemblages derived from thermodynamic simulations and validated these finding through experimental data. This approach allowed us to understand the correlation between phase assemblage and compressive strength of [CAC + FA] binders. This study also develops a novel method that evaluates the degree of reaction of FA in non-Portland cement binders. Overall, this study systematically elucidates the influences of FAs on properties of CAC. Moreover, quantification of the degree of reaction of FA in CAC binders makes this study distinguishing from others.

2. Experimental program

2.1. Materials

The CAC and 13 FAs were supplied by Almatis, USA and Boral Resources, USA, respectively. All precursors were received as powders. Chemical compositions of CAC and FAs were determined by x-ray fluorescence (Oxford X-supreme 8000). Oxide composition, density (provided by suppliers), particle size distribution (d50), and specific surface area (SSA) of CAC and FAs, are shown in Table S1 **& S2.**

2.2. Mixture design and experimental methods

In this study, CAC was used as the primary cementitious material for the binder. The replacement levels of FAs for CAC binders were $10\%_{mass}$, $20\%_{mass}$, $30\%_{mass}$, $40\%_{mass}$, and $50\%_{mass}$. The liquid-to-solid ratio of [CAC + FA] is a constant (0.5).

Isothermal microcalorimeter (TAM IV), manufactured by TA Instruments, was used to measure the heat release during the hydration of CAC binders. During the sample preparation, [CAC + FA] binders were hand mixed for 3 min before the addition of water for appropriate particle intimacy. The mixtures were then hand mixed with deionized water for 1 min and a small amount of the binder was put into a glass ampoule and sealed with Teflon cap. The microcalorimeter was maintained at 20 ± 0.2 °C for 72 h. The microcalorimeter measured the heat evolution profiles of 66 unique mixture designs (i.e., plain CAC and 65 [CAC + FA] binders).

The compressive strength of [CAC + FA] (paste samples) was tested based on ASTM C109 [38]. Binders were then casted into customized silicon cubic molds (i.e., 6 mm × 6 mm x 6 mm) and cured at > 98% relative humidity and 25 ± 0.1 °C for 3 days. After curing, the samples were taken out from the molds and were polished using sandpaper to obtain even surfaces on all sides. The compressive strength was

measured by using Instron-5881, Norwood, MA, USA. The compressive strength for each binder was calculated as the average of measurements of triplicate specimens. It should be noted that only 46 unique mixture designs were tested for compressive strength.

Particle size distribution (PSD) of all the precursors were measured using static light scattering particle analyzer (Microtrac S3500) with an assumption that all particles were spherical shape. CAC and FAs were suspended in a solution of isopropanol at 1 molarity and deionized water solution in the measurement, respectively. Ultrasonic pulses were applied to dilute suspension of powders to avoid agglomeration. The specific surface area (SSA) of FAs and CAC was determined by calculating based on the PSD values. It was assumed that all particles were smooth, with no surface roughness, and solid, without any internal porosity.

X-ray diffraction (XRD) was performed to investigate the hydrate and anhydrate phases in CAC binders. The cured specimens from compressive strength were crushed and immersed in ethanol for 24 h to stop the hydration reaction. Then samples were subjected to vacuum filtration and then dried in an oven at 60 °C for an hour. The XRD patterns were recorded on Panalytical X-Pert PRO diffractometer in standard continuous mode with a fixed divergence slit size of 0.125°. A scan step size of 0.05°2θ between the scanning range of 5°2θ to 90°2θ was utilized with a Kα1 wavelength = 1.54056 Å. The X-ray tube was conducted at a voltage of 45 kV and a current of 40 mA.

2.3. Topological constraint theory (TCT)

Topological constraint theory [35,37] is a concept that provides a framework for understanding the structural arrangement of amorphous materials (e.g., FAs). TCT refers to the restrictions imposed on the movement of atoms or molecules within a material due to their connectivity. In calcium aluminate silicate rich materials, the arrangement of calcium, aluminum, and silicon atoms plays a crucial role in determining their reactivity. TCT suggests that the presence of highly coordinated atoms, such as aluminum and silicon can increase the rigidity of the network also called as network formers, while the presence of lower coordinated atom such as calcium can decrease the rigidity of the network. In this study, all the FAs are classified into two polymerization regimes (i.e., partially depolymerized and fully polymerized) based on *number of constraints*—the metric for evaluating the reactivity of FA [39,40]. The *number of constraints* of each FA is shown in Table S2. FA-1 to 6 are classified as partially depolymerized FAs, with high amorphous phase content; while FA-7 to 13 are classified as fully polymerized FA, with high crystalline phase content. Generally, partially depolymerized FAs are more reactive than fully polymerized FAs. It should be noted that the *number of constraints* only account for CaO and SiO_2 and Al_2O_3 because they are main component determine the rigidity of chemical structure. Other oxides (e.g., Fe_2O_3 and MgO) are excluded from these calculations. Additional information on the *number of constraints* is presented in the Supplementary Information.

2.4. Thermodynamic modeling

Thermodynamic simulation is a promising tool to understand hydration products of cementitious binder. One commonly used model is Gibbs energy minimization, which enables researchers to predict the equilibrium phase assemblage at various hydration ages. In this study, thermodynamic simulations for the [CAC + FA] binders were conducted using the Gibbs Energy Minimization software [1,2,41,42], specifically GEM-Selektor v.3.7 (GEMS). GEMS is a widely used interactive package for geochemical modeling that calculates the equilibrium phase assemblage by considering the presence of various phases and species. Thermodynamic data for aqueous species and various solids were acquired from the PSI-GEMS thermodynamic database. Additionally, the solubility products for relevant phases were obtained from the Cemdata 18 database [44]. The stoichiometric chemical compositions, liquid-to-solid ratio, and curing conditions were used as the input parameters to simulate the equilibrium phase assemblage [9,45,46].

3. Results and discussion

3.1. Hydration kinetics

The heat evolution profiles for plain CAC and [CAC + 20% FA] binders at 20 °C for 3 days are shown in Fig. 1. This replacement level was selected to clearly observe the effects of FA without allowing it to overwhelmingly dominate the hydration reaction. The results clearly show that chemical compositions and molecular structures of FAs can significantly influence the hydration kinetics of CAC. Results pertaining to fully polymerized (Figs. 1**a** and 1**c**), and partially depolymerized (Figs. 1**b** and 1**d**) FAs are presented separately. This is because the two types of FAs, owing to their distinct chemical structure and dominant composition, impact the hydration kinetics of CAC via different mechanisms. As shown in Fig. 1**a**, most fully polymerized FAs shorten the induction period of CAC and cause rapid acceleration of early-age hydration of CAC; which manifests as steep slopes of the acceleration regime until the main hydration peak (i.e., when the heat flow rate is at its maximum). This is because fully polymerized FAs contain a high volume of crystalline content; and, therefore, have low dissolution rate—and a slow rate of ion release into the contiguous solution—compared to their partially depolymerized counterparts. Owing to their low reactivity, such FAs essentially act as fillers, providing an additional surface for heterogeneous nucleation of calcium aluminate hydrates; thereby accelerating CAC hydration during the early ages [43–45]. As an example of the aforementioned "filler effect": [CAC + FA-9] has the earliest occurrence and greatest intensity of heat flow rate peak; this is due to FA-9′s filler effect. Furthermore, FA-9 does not contain SO_3, which would have manifested as a delayed hydration peak due to retardation of CAC hydration. Likewise, [CAC + FA-12] features an intense heat flow peak due to FA-12′s filler effect; albeit delayed than other systems. This delay in the occurrence of the peak—or the deceleration of early-age hydration—in the [CAC + FA-12] system can be attributed to the presence of SO_3 in FA-12; which results in a burst of ettringite nucleation, followed by a slow growth of the ettringite nuclei, and ultimately a slow phase transformation of the ettringite crystals to monosulfoaluminate. Another crucial point to note is that the cumulative heat release of [CAC + FA-13] at 3 days is lower than all other pastes, including the plain CAC paste (Fig. 1**c**). This is because FA-13 has the highest *number of constraints*; and, thus, is expected to have the lowest reactivity of all FAs. Yang et al. [46] have reported that the unreacted SCMs can prevent long-term hydration of CAC by blocking the pathways for water contact. Therefore, the cumulative heat of [CAC + FA-13] could be attributed to a large amount of unreacted FA-13 obstructing CAC's access to water.

As can be seen in Fig. 1**b**, partially depolymerized FAs decelerate early-age hydration of CAC; and hydration peaks—in general—appear later than plain CAC. Due to high reactivity, partially depolymerized FAs are expected to release more ions (e.g., $H_2SiO_4^{2-}$; $Al(OH)_4^-$; Ca^{2+}; SO_4^{2-}; etc.) into pore solution. The SO_3 content in all partially depolymerized FAs is greater than $1\%_{mass}$. Consequently, the SO_4^{2-} released FAs are expected to decelerate early-age hydration of CAC. As can be seen in Fig. 1**d**, all [CAC + FA] binders release more heat at 3 days compared to that of plain CAC paste. Previous studies [1,21,47,48] have shown that reactions leading to the formation of ettringite and monosulfoaluminate release more heat compared to those producing calcium aluminate hydrates. Furthermore, the high reactivity of the partially depolymerized FAs allows them to partake in (exothermic) chemical reactions with anhydrous phases as well as hydration products; thus, resulting in the formation of additional hydration products (e.g., straetlingite) and greater cumulative heat release. It should be pointed out that the filler effect also manifests in partially depolymerized FAs; however, the magnitude of the filler effect is expected to be substantially less

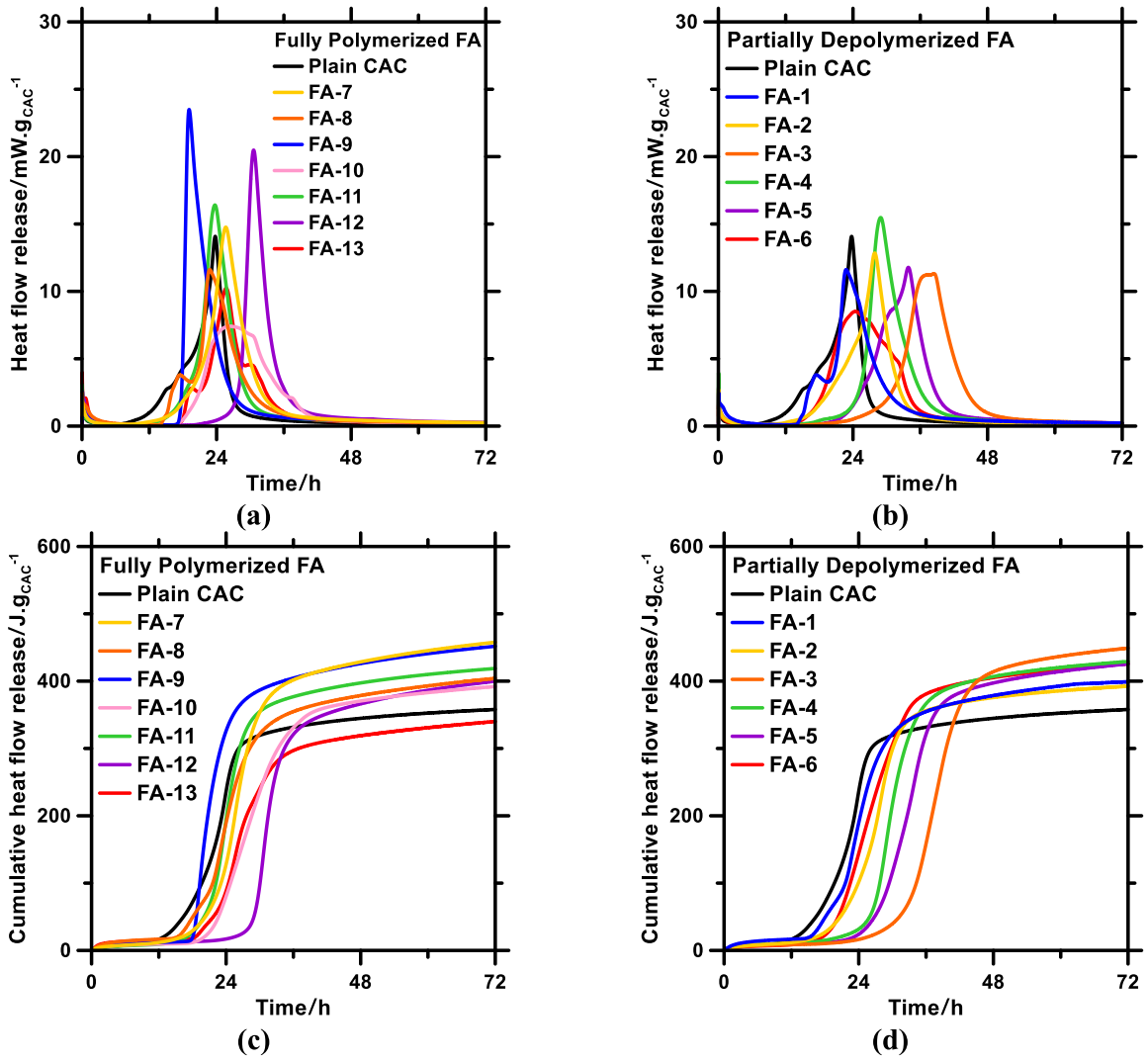

Fig. 1. [CAC+ 20% FA] binders' hydration heat release profiles obtained from isothermal calorimetry, that is, heat flow rate of **(a)** [CAC + fully polymerized FA], and **(b)** [CAC + depolymerized FA]; and cumulative heat of **(c)** [CAC + fully polymerized FA], and **(d)** [CAC + depolymerized FA]. The FA types is illustrated in the legend.

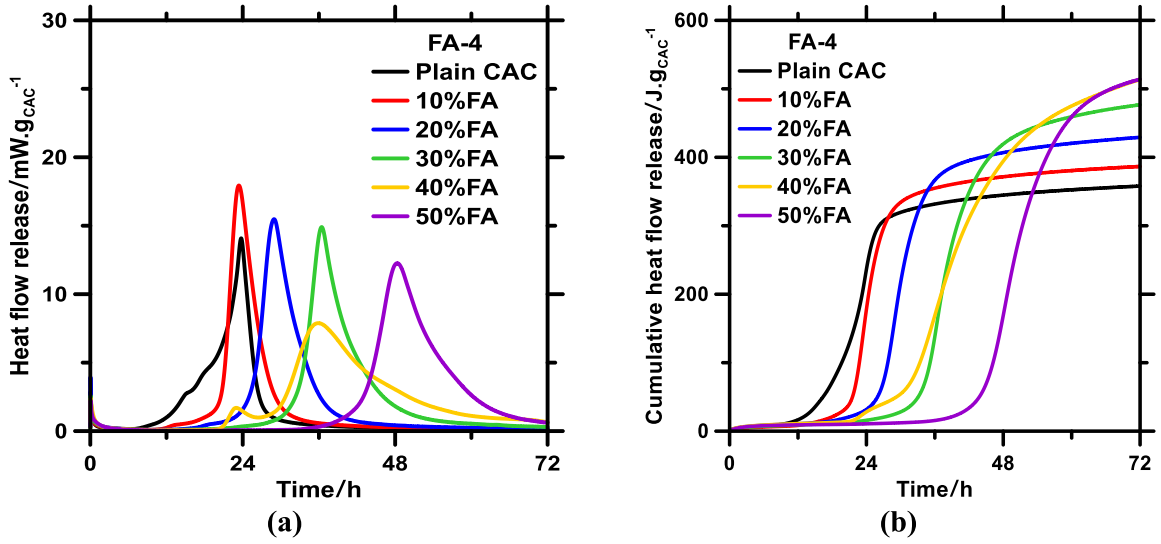

Fig. 2. [CAC + FA-4] binders' hydration heat release profiles obtained from isothermal calorimetry, that is, **(a)** heat flow rate and **(b)** cumulative heat at different replacement level. The legend indicates the replacement level.

influential than that caused by FA reactivity.

Fig. 2 exhibits heat flow rate and cumulative heat profiles of CAC replaced by FA-4 at different replacement levels. This figure indicates the impact of replacement level on the CAC hydration kinetics. [CAC + FA-4] binder is chosen as the representative binder owing to FA-4's high reactivity. In Fig. 2**a**, it can be observed that the shortest induction and highest reaction intensity is companied with CAC replaced by 10% FA. This is primarily due to the FAs filler effect. With increasing replacement level of FA-4, the intensity of the heat flow rate peak progressively decreases, the time of occurrence of the peak is delayed, and the peaks are broadened (resulting in greater cumulative heat release after ~48 h). These trends in Fig. 2 are nearly identical to those observed in [C_3A + $CaSO_4$] and [CAC + $CaSO_4$] systems with increasing $CaSO_4$ contents [1,49]. These trends in the heat evolution profiles can be explained by the progressive increase in SO_3 content of the binder with increasing replacement levels of SO_3-containing FA; which results in burst nucleation of ettringite, followed by its slow growth, and eventually the slow-but-consistent transformation of ettringite to monosulfoaluminate [50,51]. Binders with greater SO_3 content feature ettringite precipitation for longer durations; which, essentially, results in the delayed occurrence of the peak. Therefore, based on these results, it is clear that an increase in the content of SO_3-containing FAs significantly decelerates early-age hydration of CAC; resulting in delayed and broad hydration peaks, and slow-but-consistent growth of ettringite and monosulfoaluminate in lieu of calcium aluminate hydrates.

Next, we attempted to correlate the hydration kinetics of [CAC + FA] binders with the chemo-structural parameter of the FAs. Fig. 3**a** shows the correlation between cumulative heat release of [CAC + FA] binders and *number of constraints* of FAs. At first glance, no clear trend is found. To better understand the influence of *number of constraints*, the data are split based on the type (i.e., partially depolymerized; and fully polymerized) of FAs. This allows FAs in the same classification to have similar molecular structures, chemical characteristics, and overall reactivity. The correlations between cumulative heat and *number of constraints* for partially depolymerized FAs are shown in Fig. 3**b**. As can be seen, the 3-day cumulative heat is broadly unaffected by the *number of constraints* of the FAs; and this remains true for all FA replacement levels. This is because the partially depolymerized FAs are reactive; and regardless of the *number of constraints* and chemical compositions, they can release sufficient ions to form additional hydrates (e.g., ettringite; straetlingite; and monosulfoaluminate) through chemical reactions with anhydrous CAC phases and existing calcium aluminate hydrates (e.g., C_2AH_8) in the binders. Fig. 3**c** shows the cumulative heat–*number of constraints* correlation for binders formulated using fully polymerized FAs. Here, for a given value of *number of constraints*, the cumulative heat increases with FA content; this is because the additional surface area provided by FA particulates accelerates the nucleation and growth of hydrates via the filler effect. The *number of constraints* is also found to be influential in the case of fully polymerized FAs. As the *number of constraints* increases, the corresponding decrease in reactivity of the FAs results in decreasing tendency to react with anhydrous CAC phases and hydration products; thus, resulting in lower cumulative heat. Based on these analyses, a closed-form analytical model that predicts heat release of [CAC + FA] by solely utilizing replacement level and *number of constraints* is shown in **Section S2.1**.

3.2. Compressive strength

Next, we attempted to correlate the hydration kinetics of [CAC + FA] binders with their compressive strengths. Fig. 4 plots the compressive strength of [CAC + FA] against their 3-day cumulative heat release. It is worth pointing out that the unit of cumulative heat is J. g^{-1}_{water} (not J. g^{-1}_{cement}). Previous studies [52–56] have shown that compressive strength to not just a function of solid-to-solid connectivity in the material, but also the capillary porosity. By normalizing the cumulative heat by the initial water content—as opposed to the initial cement content (J. g^{-1}_{cement})—one can account for the capillary porosity in the binders at the time of mixing. Several studies [57,58] have shown that compressive strength is correlated—broadly in a linear fashion—with cumulative

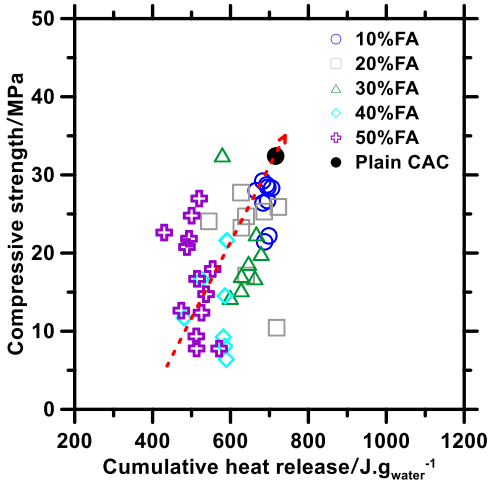

Fig. 4. Compressive strength development in [CAC+ FA] binders with respect to cumulative heat release from hydration at 3 days. The dashed line indicates the trend between cumulative heat and compressive strength.

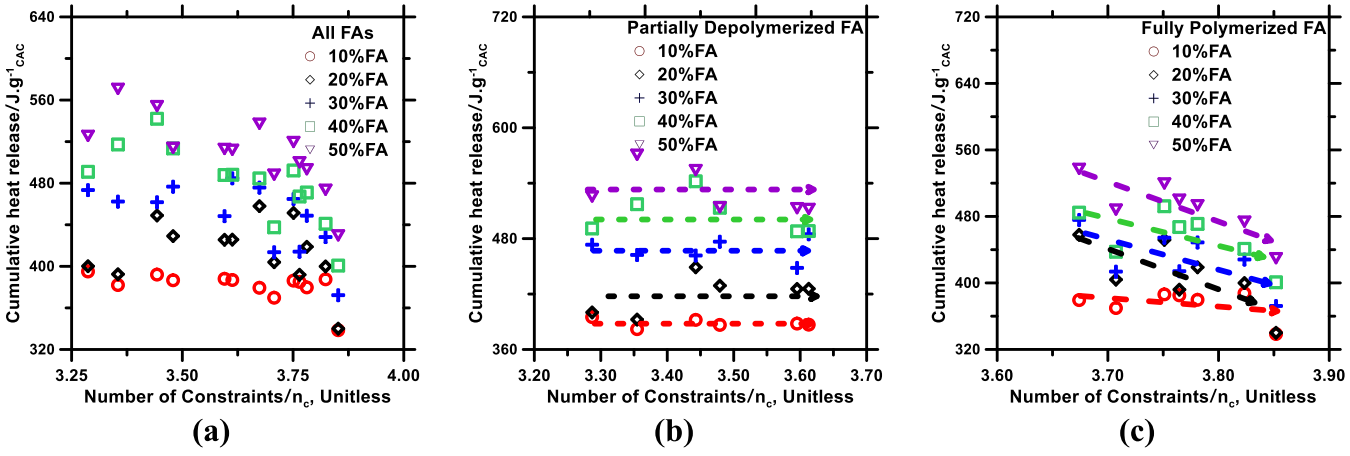

Fig. 3. Cumulative heat released from the hydration of [CAC + FA] binders plotted against the *number of constraints* of **(a)** all FAs; **(b)** partially depolymerized FAs; and **(c)** fully polymerized FAs. The dashed line indicates the general trend between *number of constraints* and cumulative heat for different FA replacement levels.

heat (normalized by water content) in PC binders. As can be seen in Fig. 4, even in [CAC + FA] binders, compressive strength increases with increasing cumulative heat; although, admittedly, this trend is not as monotonous and linear as observed in PC binders. This broadly-linear trend emerges because many factors in [CAC + FA] substantially influence both cumulative heat and compressive strength, such as complex interactions between CAC and FA, hydrates content, and solid-to-solid connectivity. If a homogenous FA type used in CAC, a clearer trend could be observed.

It should be noted that although a fraction of FA dissolves and undergoes a reaction to form hydration products (and releases heat in the process), majority of the FA remains unreacted at 3 days (see **Section 3.4** for more details). Fu et al. [59] have shown that compressive strength of cementitious binders reduces with increasing content of unreacted materials (e.g., anhydrous SCMs; aggregates) in the binders. Therefore, it could be argued that the compressive strength of [CAC + FA] binders is primarily dependent on the extent of CAC reaction, and less so on the FAs extent of reaction. In Fig. 4, it should be noted that at the replacement level of 50%$_{mass}$, [CAC + FA] binders feature a broad range of compressive strength; whereas the differences in their 3-day cumulative heat releases are comparatively minor and fall within a smaller range. Exact reasons for this discrepancy are not clear; but it can be said that at such a high replacement level of FA, its chemistry—even the oxides present in minor quantities—plays a significant role in chemical reactions, microstructural evolution, and strength development; which cannot be explained simply based on cumulative heat release [46,60,61]. That said, for FA replacement levels of 40%$_{mass}$ or lower, the cumulative heat release is a reasonably good metric for estimation of compressive strength; wherein, greater cumulative heat implies greater compressive strength, and vice versa.

Next, Fig. 5**a** demonstrates the correlation between compressive strength of [CAC + FA] binders and *number of constraints* of FAs. Similar to cumulative heat against *number of constraints* (Fig. 3**a**), no obvious trend is observed; unless the FAs are classified on the bases of their degree of polymerization. Fig. 5**b** demonstrates the compressive strength–*number of constraints* correlation of partially depolymerized FAs. Here again, independent of the replacement level, the *number of constraints* exerts little-to-no influence on compressive strength. This is because the partially depolymerized FAs have relatively higher intrinsic dissolution rates; and, regardless of their *number of constraints* and chemical compositions, can dissolve and partake in chemical reactions with other phases present in the binders. In Fig. 5**c**, the compressive strength–*number of constraints* correlations of fully polymerized FAs are more complex. At 10-to-30% replacement levels of FAs, compressive strength declines with an increase in the FAs' *number of constraints* (low reactivity). This is because fully polymerized FAs have a more rigid, networked structure; and, therefore, are less reactive, and unable to partake in chemical reactions that would lead to enhanced formation of space-filling (strength-improving) hydrates. That said, at higher replacement levels of 40%$_{mass}$ and 50%$_{mass}$, compressive strength does not decline with an increase of *number of constraints*. Reasons for this are not clear; but it is hypothesized that, in such binders, the FA becomes a dominant component of the binder, and although its reactivity is low, it can dissolve (and release siliceous and aluminate ions) and react to reasonable extents to form space-filling hydrates and contribute to strength. This would also explain why [CAC + 50% FA] binders, generally, have higher compressive strength than [CAC + 40% FA] binders. Based on these analyses, a closed-form analytical model that predicts compressive strength of [CAC + FA] by solely utilizing replacement level and *number of constraints* is shown in **Section S2.2**.

3.3. X-ray diffraction (XRD)

Results obtained from analyses of plain CAC, [CAC + 50%FA-4], and [CAC + 50%FA-13] binders by XRD are shown in Fig. 6 where, FA-4 and FA-13 are representatives of partially depolymerized and fully polymerized FA, respectively. According to crystallographic data from International Centre for Diffraction Data, the crystalline phases in XRD patterns are identified. In plain CAC binder, the main hydration products are CAH_{10} and C_2AH_8. This is expected, and in agreement with XRD patterns reported in prior studies [21,62,63]. The anhydrous phases (i.e., CA and CA_2) are also expected to appear in XRD patterns; this is because the calorimetry profile indicates the degree of reaction of CAC at 3 days is 79%. In the XRD pattern of plain CAC paste, a small amount of monosulfoaluminate is observed due to the SO_3 content in CAC. Monosulfoaluminate is also observed in all [CAC + FA] binders; this is expected because at the age of 3 days (when XRD was performed), ettringite—resulting from the reaction of SO_3 with the CA and CA_2 phases—is expected to have undergone a complete or near-complete transformation to monosulfoaluminate. In the XRD patterns of [CAC + FA] binders, the noise and weak peak intensity are observed due to the amorphous content in FAs. Peaks for quartz are attributed to crystalline SiO_2 in FAs. More straetlingite is formed in [CAC + FA-4] due to several factors: a low *number of constraints*, a partially depolymerized network structure resulting in higher reactivity, and high CaO and SiO_2 contents. Therefore, FA-4 can release sufficient calcium and silicate ions to react with free aluminate in pore solution. This result is consistent with the findings from previous studies [22,64–66]; which have reported that the Ca^{2+} and $H_2SiO_4^-$ released from FA can react with existing hydrates (i.e., CAH_{10} and C_2AH_8) and ionic species in the binder to form straetlingite at room temperature. Enhanced formation of straetlingite results in a concomitant reduction in the amount of calcium aluminate hydrates (i.

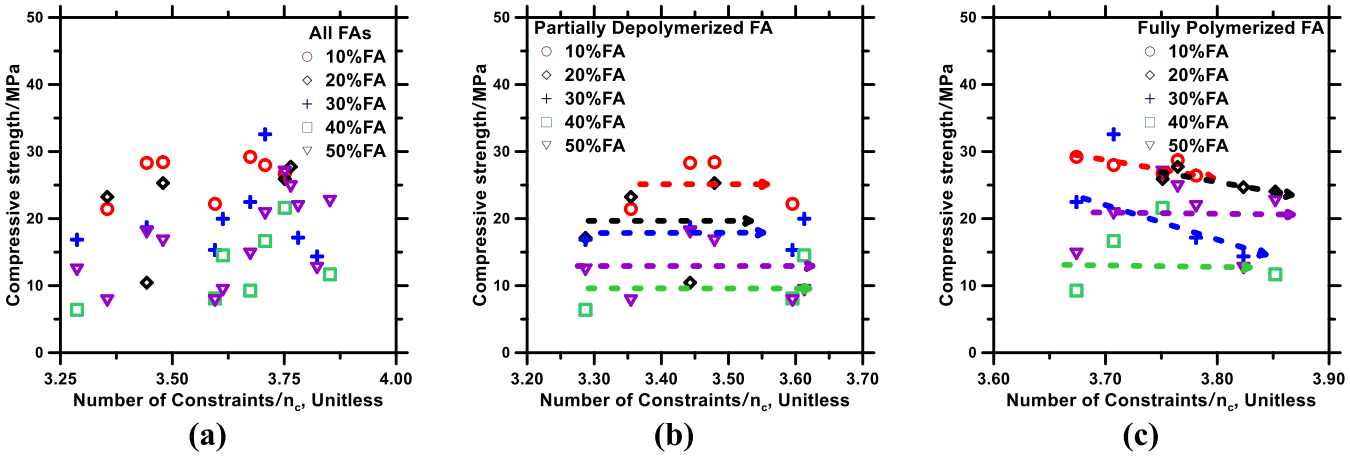

Fig. 5. Compressive strength [CAC + FA] binders at 3 days corresponding to network structure (*number of constraints*) of: **(a)** all FAs; **(b)** partially depolymerized FAs; and **(c)** fully polymerized FAs. The dashed line indicates the general trend between *number of constraints* and compressive strength at different replacement levels.

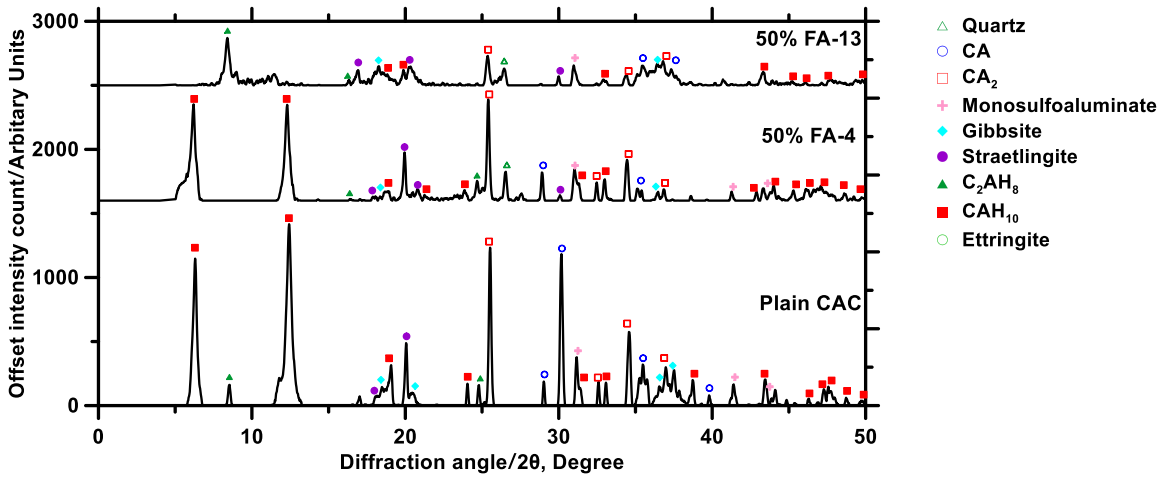

Fig. 6. X-ray diffraction patterns of **(a)** plain CAC; **(b)** [CAC + FA-4] binder; and **(c)** [CAC + FA-13] binder prepared with 0.5 water-to-solid ratio and cured for 3 days at 25 °C.

e., CAH_{10} and C_2AH_8).

3.4. Thermodynamic simulations

This section presents phase assemblages of [CAC + FA] binders obtained from thermodynamic simulations. Phase assemblages of three representative binders—the same ones evaluated by XRD in Fig. 6—are shown in Fig. 7. These phase assemblages reveal volumes of hydration products and unreacted precursors with respect to the degree of hydration of CAC or FA. In these thermodynamic simulations, the degree of hydration of CAC at 3 days was assumed to be ~79%; this value was determined from cumulative heat release of the binders at 3 days, and the standard enthalpy of hydration of CAC (*N.B.: The enthalpy of hydration of CAC was estimated from the cumulative heat release of plain CAC and several [CAC + FA] binders for 21 days; where we assumed that CAC is completely reacted at 21 days* [67–69]. *And, the degree of reaction of CAC for [CAC + FA] binders is the ratio of cumulative heat at 3 days to 21 days*). In the XRD patterns (Fig. 6), the hydration products consist of CAH_{10} phase; which is not present in the thermodynamic simulations (Fig. 7). The thermodynamic simulation of a given binder converges to form the metastable phase that has the lowest enthalpy. The formation enthalpies of C_2AH_8 and CAH_{10} are -5433 and -5320 kJ.mol^{-1} [70,71], respectively. Thus, CAH_{10} is not formed in thermodynamic simulations; and, instead, the formation of C_2AH_8 is favored. The remaining hydrates in thermodynamic simulations are consistent with those represented in the XRD patterns. In Fig. 7**a**, the dashed line indicates the phase assemblage of the binders when 79% of CAC has reacted. Compared to phase assemblages of other binders, plain CAC paste contains the smallest porosity and the largest volume fraction of hydrates (mainly C_2AH_8); which explains why it exhibits the highest compressive strength (~32 MPa). In the plain CAC paste, hydration is arrested at 87% reaction of CAC because of the depletion of water (represented by solid line). In Figs. 7**b** and 7**c**, the dashed line indicates the phase assemblage of binders and the degree of reaction at 3 days when 79% of CAC has reacted. [CAC + 50% FA-4] contains high straetlingite, which is consistent with the XRD pattern of the binder (Fig. 6). The phase assemblage of [CAC + 50% FA-13] is qualitatively similar to that of [CAC + 50% FA-4], with the exception of a lower straetlingite content in the former. This difference is attributed to the fully polymerized nature of FA-13, which leads to a high *number of constraints* and low reactivity. Furthermore, FA-13 has a relatively low Cao and SiO_2 content; all of which—as stated previously—limit chemical interaction between FA and other phases in the binder, and result in limited precipitation of straetlingite, instead favoring the formation of calcium aluminate hydrates (e.g., C_2AH_8) directly from the hydration of anhydrous CAC phases (Fig. 7**c**). We would like the point out that Figs. 8 and 9 show

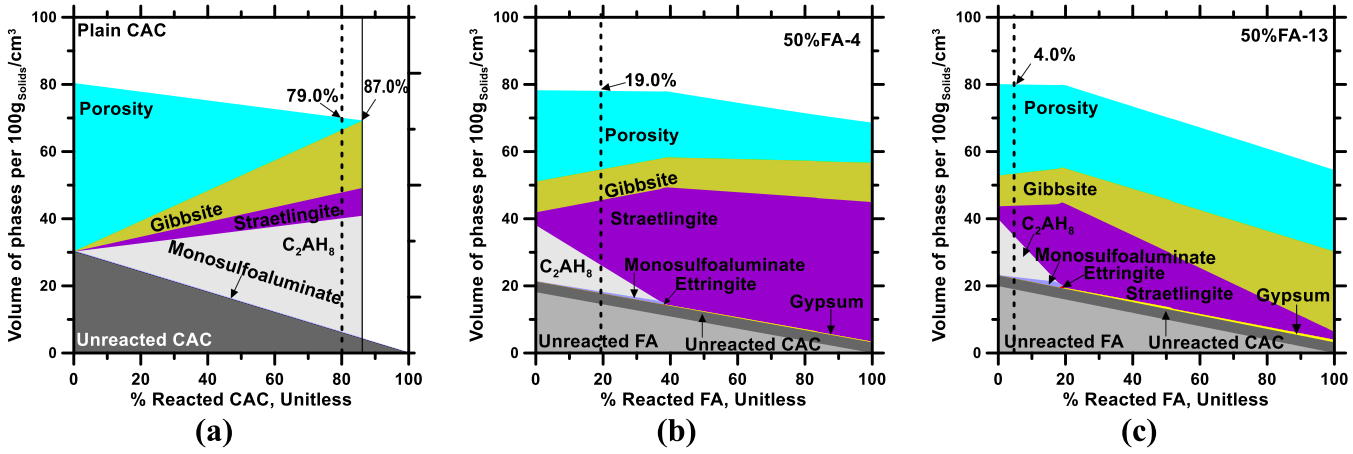

Fig. 7. Equilibrium phase assemblage of: **(a)** plain CAC; **(b)** [CAC + 50% FA-4] binder; and **(c)** [CAC + 50% FA-13] binders at 3 days as produced by thermodynamic simulations. The vertical dashed line in (b) and (c) represents the degree of hydration of FA at 3 days; which was estimated from the correlation between compressive strength and volume fraction of hydrates in the binder (see Fig. 7). Here, in all simulations including, the degree of hydration of CAC, FA-4 and FA-13 are 79%,19%, and 4%, respectively (shown as vertical dashed line); this value was obtained from the analyses of short- and long-term isothermal calorimetry experiments.

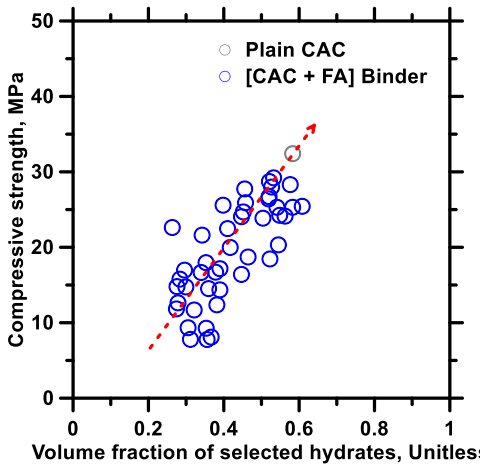

Fig. 8. The correlation between volume fraction of select hydrates and compressive strength at 3 days of [CAC + FA] binders. The FA replacement levels of [CAC + FA] binders are 10-to-50%$_{mass}$. The dashed line indicates the general trend between volume fraction of hydrates and compressive strength. This correlation was used to determine the degree of reaction of each FA at 3 days.

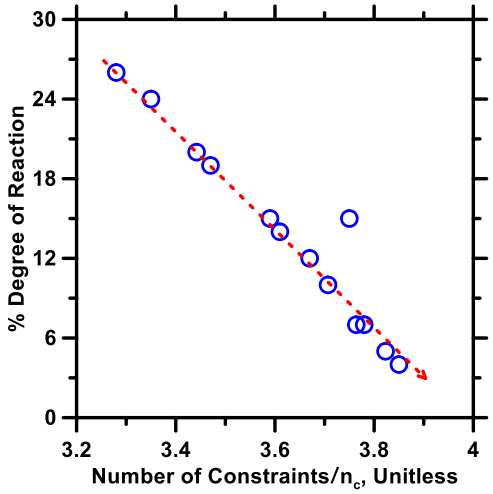

Fig. 9. A linear correlation between *number of constraints* and degree of reaction of FAs at 3 days. The dashed line indicates the linear trend between *number of constraints* and degree of reaction of FA. An important finding of this analyses: the degree of reaction of a given FA is independent of its content (%$_{mass}$) in the binder.

phase assemblages of selected [CAC + FA] binders; that said, across several other [CAC + FA] binders, reasonable agreement between XRD patterns and thermodynamic simulations was found. This agreement between experiments and thermodynamic simulations not only validates the simulations, but also allows us to further process the simulation outcomes to derive other relevant parameters pertaining to the binders (discussed below).

We attempted to correlate the phase assemblages of [CAC + FA] binders with their compressive strength; and, through such analyses, degree of reaction of FA can be estimated. Due to distinct molecular structures and chemical compositions, the degree of reaction of FAs varies over a wide range; and there are currently no well-established methods for estimating FAs' degree of reaction in non-PC systems. Generally, FAs with low *number of constraints* are reactive, and, thus, dissolve and react to a greater degree of reaction at 3 days (or other ages); and vice versa. To estimate the degree of reaction of FA at 3 days, thermodynamic simulations of [CAC + FA] binders with varying degrees of reaction of FAs—ranging from 1% to 50% with 1% increments—were simulated; while the degree of hydration of CAC was fixed at 79% (a value obtained from both short- and long-term isothermal calorimetry experiments). Previous studies [72–76] have shown that the compressive strength of cementitious binders increases monotonically with increasing volume fraction of hydrates (which scales linearly with the degree of hydration of the cementitious materials). This is because the volume fraction of hydrates is a crude measure of solid-to-solid connectivity and porosity—and, thus, of mechanical properties—of a given cementitious binder. In this study, for [CAC + FA] binders, calcium aluminate hydrates (e.g., C_2AH_8) and straetlingite—the major hydrates—were assumed to be the primary phases that provide strength; while other phases—given their low volume fraction in the binder at 3 days (e.g., monosulfoaluminate; see Fig. 7)—were assumed to not contribute significantly to compressive strength [46,60,61]. Next, the volume fraction of calcium aluminate hydrates and straetlingite (after 3 days of hydration) at various reactivity of FAs were plotted against compressive strength; and, in our analyses, separate plots were generated for each degree of reaction of FA. Through analyses of the correlations between volume fraction of hydrates and compressive strength, the best *near-linear* correlation that was obtained is shown in Fig. 8. Here, as expected, the compressive strength monotonically increases with volume fraction of hydrates; and, based on this correlation, the degree of reaction of FA in each [CAC + FA] binder was determined. The trend is broad because this figure cannot account for other factors (e.g., fineness; minor compositions in FAs; etc.) that can affect the compressive strength.

The degree of reaction of FAs, thus obtained, with respect to the FAs' *number of constraints* is shown in Fig. 9. An important finding of this analysis is that the degree of reaction of a given FA is independent of its content in the binder. As an example, the degree of reaction of FA-4 in [CAC + 10% FA-4] and in [CAC + 40% FA-4] are found to be within ± 4%. In fact, this independence of FAs degree of reaction from its content in the binder was found to be true for all FAs examined in this study, regardless of the FAs' chemical compositions and *number of constraints*. As can be seen in Fig. 9, the degree of reaction of FA at 3 days monotonically decreases with an increase in *number of constraints*. This is expected; because higher *number of constraints* imply lower reactivity of FA. Across all [CAC + FA] binders, FAs were found to have degrees of reaction (a 3 days) ranging from ~5% to ~25%; which is also in agreement with prior studies [30,39,77]. The FA-9 type deviates from the prevailing pattern, an anomaly attributed to the limitations of *number of constraints*. While *number of constraints* is an indirect measurement to estimate the amorphous content in FAs. However, certain FAs might possess substantial silica or aluminate content yet still display a high level of amorphous content. A more accurate assessment of amorphous content can be obtained by using XRD, which demands advanced analytical competencies. The primary objective of this study, however, is to employ an inexpensive and simple method to estimate the reactivity of FA. As such, the presence of this exceptional FA is acceptable within the scope of this research.

4. Conclusions

This paper investigated the influences of FA on hydration kinetics, compressive strength, and phase assemblage of [CAC + FA] binders. 13 FAs, each with distinct chemical composition and molecular structure, were used to partially substitute CAC. Chemical composition of each FA was used to obtain a singular chemo-structural attribute, that is, the *number of constraints*, as a proxy to its reactivity in pore solutions. FAs could be classified as: fully polymerized (low reactivity); or partially depolymerized (high reactivity). Furthermore, thermodynamic simulations and XRD were employed to correlate the phase assemblages of [CAC + FA] binders with their compressive strengths; and, to estimate the reactivity of FAs. This is first study to develop a method that evaluates the reactivity of FA in non-PC binders.

Results from heat evolution profiles demonstrated that additional surfaces from FAs. accelerated early-age hydration of CAC. FAs with high SO_3 content decelerated early-age hydration of CAC; resulting in delayed occurrence and broadening of the main hydration peak. FAs with a lower *number of constraints* (and, thus, high reactivity) were found to react with anhydrous phases and hydration products to produce additional hydration products (e.g., straetlingite), which resulted in increased exothermic heat release. Results from XRD and thermodynamic simulations showed that the primary hydrates of [CAC + FA] binders are CAH_{10}, C_2AH_8, gibbsite, straetlingite, and monosulfoaluminate. In [CAC + FA] binders, the siliceous ions released from FAs result in the formation of straetlingite in lieu of calcium aluminate hydrates. The formation of straetlingite was found to be favored in binders containing FAs with low *number of constraints* (high reactivity) and high CaO- and SiO_2-contents. Thermodynamic simulations correlated with compressive strength were used to estimate the degree of reaction of FA at 3 days. It was found that the degree of reaction of common FAs ranging from ~5% to ~25% at 3 days. In [CAC + FA] binders, the degree of reaction of FA monotonically decreases with an increase in *number of constraints*.

In conclusion, this research provides a thorough investigation into the influence of common FA on the hydration kinetics and compressive strength of sustainable CAC binders. The methods for evaluating the reactivity of FA provide a solid guideline for using FA in non-PC binders. These findings offer valuable insights for future studies in sustainable cementitious binder made from FA.

CRediT authorship contribution statement

Kumar Aditya: Conceptualization, Funding acquisition, Writing – review & editing. **Neithalath Narayanan:** Funding acquisition, Supervision, Writing – review & editing. **Sant Gaurav:** Funding acquisition, Supervision, Writing – review & editing. **Ponduru Sai Akshay:** Formal analysis, Investigation, Methodology, Writing – original draft. **Huang Jie:** Funding acquisition, Supervision, Writing – review & editing. **Han Taihao:** Formal analysis, Investigation, Writing – original draft.

Declaration of Competing Interest

The authors declare that they have no known competing financial interests or personal relationships that could have appeared to influence the work reported in this paper.

Data Availability

Data will be made available on request.

Acknowledgement

The authors acknowledge financial support from the Kummer Institute (Missouri S&T) Ignition Grant; the National Science Foundation (NSF-CMMI: 1932690); and the Federal Highway Administration (Award no: 693JJ31950021).

Appendix A. Supporting information

Supplementary data associated with this article can be found in the online version at doi:10.1016/j.conbuildmat.2024.135062.

References

[1] J. Lapeyre, S.A. Ponduru, M. Okoronkwo, H. Ma, A. Kumar, Hydration of high-alumina calcium aluminate cements with carbonate and sulfate additives, J. Therm. Anal. Calorim. 147 (2022) 5575–5587, https://doi.org/10.1007/s10973-021-10939-4.

[2] S.A. Ponduru, T. Han, J. Huang, A. Kumar, Predicting compressive strength and hydration products of calcium aluminate cement using data-driven approach, Materials 16 (2023) 654, https://doi.org/10.3390/ma16020654.

[3] J.F. Zapata, A. Azevedo, C. Fontes, S.N. Monteiro, H.A. Colorado, Environmental impact and sustainability of calcium aluminate cements, Sustainability 14 (2022) 2751, https://doi.org/10.3390/su14052751.

[4] J. Bizzozero, Hydration and dimensional stability of calcium aluminate cement based systems, EPFL (2014), https://doi.org/10.5075/epfl-thesis-6336.

[5] H. Pöllmann, Calcium aluminate cements – raw materials, differences, hydration and properties, Rev. Mineral. Geochem. 74 (2012) 1–82, https://doi.org/10.2138/rmg.2012.74.1.

[6] R.J. Mangabhai, ed., Calcium Aluminate Cements: Proceedings of a Symposium dedicated to H G Midgley, London, July 1990, CRC Press, London, 2014. https://doi.org/10.1201/9781482288872.

[7] K.E. Kurtis, Innovations in cement-based materials: addressing sustainability in structural and infrastructure applications, MRS Bull. 40 (2015) 1102–1109, https://doi.org/10.1557/mrs.2015.279.

[8] H. Kim, H.M. Son, H.K. Lee, Review on recent advances in securing the long-term durability of calcium aluminate cement (CAC)-based systems, Funct. Compos. Struct. 3 (2021) 035002, https://doi.org/10.1088/2631-6331/ac1913.

[9] K. Scrivener, A. Capmas, 13 – Calcium Aluminate Cements, in: 1998. https://doi.org/10.1016/B978–075066256-7/50025–4.

[10] A. Engbert, S. Gruber, J. Plank, The effect of alginates on the hydration of calcium aluminate cement, Carbohydr. Polym. 236 (2020) 116038, https://doi.org/10.1016/j.carbpol.2020.116038.

[11] B. Lothenbach, L. Pelletier-Chaignat, F. Winnefeld, Stability in the system CaO–Al2O3–H2O, Cem. Concr. Res. 42 (2012) 1621–1634, https://doi.org/10.1016/j.cemconres.2012.09.002.

[12] G. Bernardo, A. Telesca, G.L. Valenti, A porosimetric study of calcium sulfoaluminate cement pastes cured at early ages, Cem. Concr. Res. 36 (2006) 1042–1047, https://doi.org/10.1016/j.cemconres.2006.02.014.

[13] E. Sakai, T. Sugiyama, T. Saito, M. Daimon, Mechanical properties and microstructures of calcium aluminate based ultra high strength cement, Cem. Concr. Res. 40 (2010) 966–970, https://doi.org/10.1016/j.cemconres.2010.01.001.

[14] A.J. Majumdar, B. Singh, Properties of some blended high-alumina cements, Cem. Concr. Res. 22 (1992) 1101–1114, https://doi.org/10.1016/0008-8846(92)90040-3.

[15] M. Izquierdo, X. Querol, Leaching behaviour of elements from coal combustion fly ash: An overview, Int. J. Coal Geol. 94 (2012) 54–66, https://doi.org/10.1016/j.coal.2011.10.006.

[16] V. Sibanda, S. Ndlovu, G. Dombo, A. Shemi, M. Rampou, Towards the utilization of fly ash as a feedstock for smelter grade alumina production: a review of the developments, J. Sustain. Metall. 2 (2016) 167–184, https://doi.org/10.1007/s40831-016-0048-6.

[17] The Brainy Insights, Fly Ash Market Size by Type (Class C and Class F), Application (Cement and Concrete, Waste Stabilization, Oilfield Service, Fills and Embankments, Mining, Road Stabilization and Others), Global Industry Analysis, Share, Growth, Trends, and Forecast 2023 to 2032, The Brainy Insights, India, 2023. https://www.thebrainyinsights.com/report/fly-ash-market-13417.

[18] C. Belviso, State-of-the-art applications of fly ash from coal and biomass: a focus on zeolite synthesis processes and issues, Prog. Energy Combust. Sci. 65 (2018) 109–135, https://doi.org/10.1016/j.pecs.2017.10.004.

[19] S. Wang, T. Terdkiatburana, M.O. Tadé, Single and co-adsorption of heavy metals and humic acid on fly ash, Sep. Purif. Technol. 58 (2008) 353–358, https://doi.org/10.1016/j.seppur.2007.05.009.

[20] U. Bhattacharjee, T.C. Kandpal, Potential of fly ash utilisation in India, Energy 27 (2002) 151–166, https://doi.org/10.1016/S0360-5442(01)00065-2.

[21] H.M. Son, S. Park, H.Y. Kim, J.H. Seo, H.K. Lee, Effect of CaSO4 on hydration and phase conversion of calcium aluminate cement, Constr. Build. Mater. 224 (2019) 40–47, https://doi.org/10.1016/j.conbuildmat.2019.07.004.

[22] H.M. Son, S.M. Park, J.G. Jang, H.K. Lee, Effect of nano-silica on hydration and conversion of calcium aluminate cement, Constr. Build. Mater. 169 (2018) 819–825, https://doi.org/10.1016/j.conbuildmat.2018.03.011.

[23] O. Bayat, Characterisation of Turkish fly ashes, Fuel 77 (1998) 1059–1066, https://doi.org/10.1016/S0016-2361(97)00274-3.

[24] B. Guan, W. Lou, Q. Ye, H. Fu, Z. Wu, Calorimetric study of calcium aluminate cement blended with flue gas desulfurization gypsum, J. Therm. Anal. Calorim. 98 (2009) 737, https://doi.org/10.1007/s10973-009-0107-3.

[25] J. Bizzozero, C. Gosselin, K.L. Scrivener, Expansion mechanisms in calcium aluminate and sulfoaluminate systems with calcium sulfate, Cem. Concr. Res. 56 (2014) 190–202, https://doi.org/10.1016/j.cemconres.2013.11.011.

[26] A. Hidalgo López, J.L. García Calvo, J. García Olmo, S. Petit, M.C. Alonso, Microstructural evolution of calcium aluminate cements hydration with silica fume and fly ash additions by scanning electron microscopy, and mid and near-infrared spectroscopy, J. Am. Ceram. Soc. 91 (2008) 1258–1265, https://doi.org/10.1111/j.1551-2916.2008.02283.x.

[27] B. Pacewska, I. Wilińska, M. Nowacka, Studies on the influence of different fly ashes and Portland cement on early hydration of calcium aluminate cement, J. Therm. Anal. Calorim. 106 (2011) 859–868, https://doi.org/10.1007/s10973-011-1570-1.

[28] S. Auer, H.-J. Kuzel, H. Pöllmann, F. Sorrentino, Investigation on MSW fly ash treatment by reactive calcium aluminates and phases formed, Cem. Concr. Res. 25 (1995) 1347–1359, https://doi.org/10.1016/0008-8846(95)00127-X.

[29] C09 Committee, C618-15 Standard Specification for Coal Fly Ash and Raw or Calcined Natural Pozzolan for Use in Concrete, ASTM International, West Conshohocken, PA, 2015, https://doi.org/10.1520/C0618-15.

[30] Y. Song, K. Yang, J. Chen, K. Wang, G. Sant, M. Bauchy, Machine learning enables rapid screening of reactive fly ashes based on their network topology, ACS Sustain. Chem. Eng. 9 (2021) 2639–2650, https://doi.org/10.1021/acssuschemeng.0c06978.
[31] T. Oey, J. Timmons, P. Stutzman, J.W. Bullard, M. Balonis, M. Bauchy, G. Sant, An improved basis for characterizing the suitability of fly ash as a cement replacement agent, J. Am. Ceram. Soc. 100 (2017) 4785–4800, https://doi.org/10.1111/jace.14974.
[32] J.C. Hower, M. Mastalerz, An approach toward a combined scheme for the petrographic classification of fly ash, Energy Fuels 15 (2001) 1319–1321, https://doi.org/10.1021/ef010146z.
[33] S.V. Vassilev, C.G. Vassileva, Methods for characterization of composition of fly ashes from coal-fired power stations: a critical overview, Energy Fuels 19 (2005) 1084–1098, https://doi.org/10.1021/ef049694d.
[34] C.R. Ward, D. French, Determination of glass content and estimation of glass composition in fly ash using quantitative X-ray diffractometry, Fuel 85 (2006) 2268–2277, https://doi.org/10.1016/j.fuel.2005.12.026.
[35] J.C. Mauro, Topological constraint theory of glass, Am. Ceram. Soc. Bull. 90 (2011) 31–37.
[36] J.C. Phillips, Topology of covalent non-crystalline solids I: short-range order in chalcogenide alloys, J. Non-Cryst. Solids 34 (1979) 153–181, https://doi.org/10.1016/0022-3093(79)90033-4.
[37] K. Yang, Y. Hu, Z. Li, N.M.A. Krishnan, M.M. Smedskjaer, C.G. Hoover, J.C. Mauro, G. Sant, M. Bauchy, Analytical model of the network topology and rigidity of calcium aluminosilicate glasses, J. Am. Ceram. Soc. 104 (2021) 3947–3962, https://doi.org/10.1111/jace.17781.
[38] ASTM International, C109/C109M-20b Standard Test Method for Compressive Strength of Hydraulic Cement Mortars (Using 2-in. or [50-mm] Cube Specimens), ASTM International,, 2020, https://doi.org/10.1520/C0109_C0109M–20B.
[39] R. Bhat, T. Han, S. Akshay Ponduru, A. Reka, J. Huang, G. Sant, A. Kumar, Predicting compressive strength of alkali-activated systems based on the network topology and phase assemblages using tree-structure computing algorithms, Constr. Build. Mater. 336 (2022) 127557, https://doi.org/10.1016/j.conbuildmat.2022.127557.
[40] T. Han, R. Bhat, S.A. Ponduru, A. Sarkar, J. Huang, G. Sant, H. Ma, N. Neithalath, A. Kumar, Deep learning to predict the hydration and performance of fly ash-containing cementitious binders, Cem. Concr. Res. 165 (2023) 107093, https://doi.org/10.1016/j.cemconres.2023.107093.
[41] D. Torrens-Martín, F. Winnefeld, L.J. Fernández-Carrasco, Thermodynamic model for ternary OPC/CAC/Calcium Sulfate binders, Constr. Build. Mater. 302 (2021) 124120, https://doi.org/10.1016/j.conbuildmat.2021.124120.
[42] B. Lothenbach, D.A. Kulik, T. Matschei, M. Balonis, L. Baquerizo, B. Dilnesa, G. D. Miron, R.J. Myers, Cemdata18: A chemical thermodynamic database for hydrated Portland cements and alkali-activated materials, Cem. Concr. Res. 115 (2019) 472–506, https://doi.org/10.1016/j.cemconres.2018.04.018.
[43] R. Cook, H. Ma, A. Kumar, The Effects of Various Filler Types and Size Classification on Early Hydration of C3S Poster, (2019). https://cies.mst.edu/conference/.
[44] A. Kumar, T. Oey, G. Falzone, J. Huang, M. Bauchy, M. Balonis, N. Neithalath, J. Bullard, G. Sant, The filler effect: The influence of filler content and type on the hydration rate of tricalcium silicate, J. Am. Ceram. Soc. 100 (2017) 3316–3328, https://doi.org/10.1111/jace.14859.
[45] G. Puerta-Falla, A. Kumar, L. Gomez-Zamorano, M. Bauchy, N. Neithalath, G. Sant, The influence of filler type and surface area on the hydration rates of calcium aluminate cement, Constr. Build. Mater. 96 (2015) 657–665, https://doi.org/10.1016/j.conbuildmat.2015.08.094.
[46] H.J. Yang, K.Y. Ann, M.S. Jung, Development of strength for calcium aluminate cement mortars blended with GGBS, Adv. Mater. Sci. Eng. 2019 (2019) e9896012, https://doi.org/10.1155/2019/9896012.
[47] G. Le Saoût, B. Lothenbach, P. Taquet, H. Fryda, F. Winnefeld, Hydration of calcium aluminate cement blended with anhydrite, Adv. Cem. Res. 30 (2018) 24–36, https://doi.org/10.1680/jadcr.17.00045.
[48] B. Lothenbach, D.A. Kulik, T. Matschei, M. Balonis, L. Baquerizo, B. Dilnesa, G. D. Miron, R.J. Myers, Cemdata18: A chemical thermodynamic database for hydrated Portland cements and alkali-activated materials, Cem. Concr. Res. 115 (2019) 472–506, https://doi.org/10.1016/j.cemconres.2018.04.018.
[49] J. Lapeyre, H. Ma, M.U. Okoronkwo, G. Sant, A. Kumar, Influence of Water Activity on Hydration of Tricalcium Aluminate-Calcium Sulfate Systems, J. Am. Ceram. Soc. 103 (2020) 3851–3870, https://doi.org/10.1111/jace.17046.
[50] H.F. Taylor, Cement chemistry, Thomas Telford,, 1997.
[51] W. Kurdowski, Cement and concrete chemistry, Springer, Dordrecht, New York, 2014.
[52] X. Chen, S. Wu, J. Zhou, Influence of porosity on compressive and tensile strength of cement mortar, Constr. Build. Mater. 40 (2013) 869–874, https://doi.org/10.1016/j.conbuildmat.2012.11.072.
[53] C. Lian, Y. Zhuge, S. Beecham, The relationship between porosity and strength for porous concrete, Constr. Build. Mater. 25 (2011) 4294–4298, https://doi.org/10.1016/j.conbuildmat.2011.05.005.
[54] S. Popovics, New formulas for the prediction of the effect of porosity on concrete strength, J. Am. Concr. Inst. 82 (1985) 136–146.
[55] L. Li, M. Aubertin, A general relationship between porosity and uniaxial strength of engineering materials, Can. J. Civ. Eng. 30 (2003) 644–658, https://doi.org/10.1139/l03-012.
[56] D.M. ROY, G.R. GOUDA, Porosity-strength relation in cementitious materials with very high strengths, J. Am. Ceram. Soc. 56 (1973) 549–550, https://doi.org/10.1111/j.1151-2916.1973.tb12410.x.
[57] I. Mehdipour, A. Kumar, K.H. Khayat, Rheology, hydration, and strength evolution of interground limestone cement containing PCE dispersant and high volume supplementary cementitious materials, Mater. Des. 127 (2017) 54–66, https://doi.org/10.1016/j.matdes.2017.04.061.
[58] B. Lothenbach, G. Le Saout, E. Gallucci, K. Scrivener, Influence of limestone on the hydration of Portland cements, Cem. Concr. Res. 38 (2008) 848–860, https://doi.org/10.1016/j.cemconres.2008.01.002.
[59] T.C. Fu, W. Yeih, J.J. Chang, R. Huang, The Influence of Aggregate Size and Binder Material on the Properties of Pervious Concrete, Adv. Mater. Sci. Eng. 2014 (2014) e963971, https://doi.org/10.1155/2014/963971.
[60] N.Y. Mostafa, Z.I. Zaki, O.H. Abd Elkader, Chemical activation of calcium aluminate cement composites cured at elevated temperature, Cem. Concr. Compos. 34 (2012) 1187–1193, https://doi.org/10.1016/j.cemconcomp.2012.08.002.
[61] Ö. Kırca, İ. Özgür Yaman, M. Tokyay, Compressive strength development of calcium aluminate cement–GGBFS blends, Cem. Concr. Compos. 35 (2013) 163–170, https://doi.org/10.1016/j.cemconcomp.2012.08.016.
[62] L. Fernández-Carrasco, E. Vázquez, Reactions of fly ash with calcium aluminate cement and calcium sulphate, Fuel 88 (2009) 1533–1538, https://doi.org/10.1016/j.fuel.2009.02.018.
[63] J. Goergens, T. Manninger, F. Goetz-Neunhoeffer, In-situ XRD study of the temperature-dependent early hydration of calcium aluminate cement in a mix with calcite, Cem. Concr. Res. 136 (2020) 106160, https://doi.org/10.1016/j.cemconres.2020.106160.
[64] B. Pacewska, M. Nowacka, V. Antonovič, M. Aleknevičius, Investigation of early hydration of high aluminate cement-based binder at different ambient temperatures, J. Therm. Anal. Calorim. 109 (2012) 717–726, https://doi.org/10.1007/s10973-012-2233-6.
[65] J. Ding, Y. Fu, J.J. Beaudoin, Strätlingite formation in high alumina cement - silica fume systems: Significance of sodium ions, Cem. Concr. Res. 25 (1995) 1311–1319, https://doi.org/10.1016/0008-8846(95)00124-U.
[66] J. Ding, Y. Fu, J.J. Beaudoin, Strätlingite formation in high-alumina cement — zeolite systems, Adv. Cem. Res. 7 (1995) 171–178, https://doi.org/10.1680/adcr.1995.7.28.171.
[67] S. Skalamprinos, I. Galan, T. Hanein, F. Glasser, Enthalpy of formation of ye'elimite and ternesite, J. Therm. Anal. Calorim. 131 (2018) 2345–2359, https://doi.org/10.1007/s10973-017-6751-0.
[68] W. Meng, P. Lunkad, A. Kumar, K. Khayat, Influence of silica fume and polycarboxylate ether dispersant on hydration mechanisms of cement, J. Phys. Chem. C 120 (2016) 26814–26823, https://doi.org/10.1021/acs.jpcc.6b08121.
[69] J. Lapeyre, A. Kumar, Influence of pozzolanic additives on hydration mechanisms of tricalcium silicate, J. Am. Ceram. Soc. 101 (2018) 3557–3574, https://doi.org/10.1111/jace.15518.
[70] B. Lothenbach, T. Matschei, G. Möschner, F.P. Glasser, Thermodynamic modelling of the effect of temperature on the hydration and porosity of Portland cement, Cem. Concr. Res. 38 (2008) 1–18, https://doi.org/10.1016/j.cemconres.2007.08.017.
[71] T. Matschei, B. Lothenbach, F.P. Glasser, Thermodynamic properties of Portland cement hydrates in the system CaO–Al2O3–SiO2–CaSO4–CaCO3–H2O, Cem. Concr. Res. 37 (2007) 1379–1410, https://doi.org/10.1016/j.cemconres.2007.06.002.
[72] D. Lootens, D.P. Bentz, On the relation of setting and early-age strength development to porosity and hydration in cement-based materials, Cem. Concr. Compos 68 (2016) 9–14, https://doi.org/10.1016/j.cemconcomp.2016.02.010.
[73] M. Zalzale, P.J. McDonald, Lattice Boltzmann simulations of the permeability and capillary adsorption of cement model microstructures, Cem. Concr. Res. 42 (2012) 1601–1610.
[74] M. Zalzale, P.J. McDonald, K.L. Scrivener, A 3D lattice Boltzmann effective media study: understanding the role of CSH and water saturation on the permeability of cement paste, Model. Simul. Mater. Sci. Eng. 21 (2013) 085016.
[75] A. Banala, A. Kumar, Numerical simulations of permeability of plain and blended cement pastes, Int. J. Adv. Eng. Sci. Appl. Math. 9 (2017) 67–86, https://doi.org/10.1007/s12572-017-0184-7.
[76] T. Han, S.A. Ponduru, R. Cook, J. Huang, G. Sant, A. Kumar, A deep learning approach to design and discover sustainable cementitious binders: strategies to learn from small databases and develop closed-form analytical models, Front. Mater. 8 (2022) 796476, https://doi.org/10.3389/fmats.2021.796476.
[77] T. Oey, A. Kumar, I. Pignatelli, Y. Yu, N. Neithalath, J.W. Bullard, M. Bauchy, G. Sant, Topological controls on the dissolution kinetics of glassy aluminosilicates, J. Am. Ceram. Soc. 100 (2017) 5521–5527, https://doi.org/10.1111/jace.15122.